Supporting Information

Electrochemical Aldehydes Hydrogenation: Probing the Inner-Sphere Strategy with Nickel-Bipyridine Complexes

Gabriel Durin,[‡a,b] Mijung Lee,[‡a] Martina A. Pogany,[‡a] Christian Kahl,[a] Thomas Weyhermüller,[a] Walter Leitner,[a,c] Nicolas Kaeffer[a]*

[a]Max Planck Institute for Chemical Energy Conversion, Stiftstrasse 34-36, 45470 Mülheim an der Ruhr, Germany
[b]Université Grenoble Alpes, DCM, CNRS, 38000 Grenoble, France
[c]Institut für Technische und Makromolekulare Chemie, RWTH Aachen University, Worringerweg 2, 52074 Aachen, Germany

*Corresponding author: Nicolas Kaeffer (nicolas.kaeffer@cec.mpg.de)

1. General consideration

Synthetic manipulations were performed under inert conditions of argon atmosphere either in an MBRAUN UNILAB Plus glove box or using standard Schlenk techniques, in oven-dried glassware. Organic solvents (analytical grade; Carl Roth) other than DMF were dried and degassed by passage over an MBRAUN SPS-7 solvent purification system, handled under argon atmosphere and stored over molecular sieves. 2,2-Bipyridine (≥99%) and trimethylsilyl trifluoromethanesulfonate (TMSOTf) (≥99%) were purchased from Aesar (Germany) and N,N-Dimethylformamide (DMF, 99.8%, Extra Dry over Molecular Sieve) was obtained from ACROS Organics. Tetrabutylammonium hexafluorophosphate (nBu$_4$NPF$_6$) (for electrochemical analysis, ≥99%), benzaldehyde (**S1**) (≥99%), benzoic acid (BzOH) (≥99.5%), deuterated benzoic acid (BzOD) (≥ atom 99% D), scandium(III) triflate (Sc(OTf)$_3$) (≥99%) and triethylborane solution 0.1 M in hexane (BEt$_3$) were all purchased from Merck (Darmstadt, Germany). [Ni(COD)$_2$] (98%), 4,4-bis(trifluoromethyl)-2,2'-bipyridine (≥99%) and 4,4-dimethoxy-2,2'-bipyridine (≥99%) were obtained from ABCR GmbH. NMR solvents were degassed by three freeze-pump-thaw cycles and dried over molecular sieves. [Ni(bpy)(OBz)$_2$] (**2**) was prepared according to literature procedure.[1]

^{1}H NMR spectra were acquired using Bruker AVANCE NEO 400 MHz and 500 MHz spectrometers at 298 K. ^{1}H NMR spectrum at 243 K was recorded on a Bruker AVANCE III NEO 500 MHz spectrometer equipped with prodigy cryoplatform. Chemical shifts were reported in parts per million (ppm), referenced to the residual solvent peak (DMF-d_7, δ(^{1}H) = 8.03 ppm, δ(^{13}C) = 163.15 ppm; DMSO-d_6, δ(^{1}H) = 2.50 ppm, δ(^{13}C) = 39.52 ppm) or to 0 ppm for tetramethylsilane (TMS). Coupling constants (J) are expressed in hertz. First-order spin multiplicities are abbreviated as singlet (s), doublet (d), triplet (t), and quadruplet (q). Couplings of higher-order or overlapped signals are denoted as m (multiplet). ^{13}C NMR spectra were recorded on a Bruker Avance NEO (125 MHz) spectrometer with broadband decoupling. Chemical shifts for ^{13}C NMR were referenced to the central peak of the DMSO-d_6 septet at 39.52 ppm.

IR spectra were recorded in the glovebox, using a Bruker FT-IR spectrometer (ALPHA II, PLATINUM-ATR mounted with diamond crystal) equipped with a standard KBr beam splitter.

2. Synthesis and characterizations of 2

2.1. Synthesis of [Ni(bpy)(PhCHO)] (2)

In the glovebox, [Ni(COD)$_2$] (100 mg, 364 µmol, 1.00 eq) and 2,2'-bipyridine (56.8 mg, 364 µmol, 1.00 eq) were dissolved in 2.5 mL of THF within a Schlenk tube. The color of the solution changes immediately from light yellow to dark purple. After stirring for 0.5 h, benzaldehyde (**S1**) (45.0 µl, 546 µmol, 1.50 eq) was added dropwise, resulting in the formation of a dark green precipitate. The reaction mixture was then cooled to – 38 °C for 2 h to maximize precipitation. Afterwards, the volatile solvent was removed under vacuum, and the dark residue was collected. The residue was washed with diethyl ether and dried under vacuum to yield a dark green powder (98 mg, 84 % yield). The synthesis of this complex from [Ni(bpy)(COD)] has been previously documented in the literature but, to our knowledge, NMR analysis has not been reported.[2]

^{1}H-NMR (DMSO-d_6, 500 MHz, 298 K): δ = 8.88 (d, J = 5.35 Hz, 2H, bpy 6/6'), 8.25 (d, J = 8 Hz, 2H, bpy 3/3'), 8.13 (m, 2H, bpy 4/4'), 7.55 (m, 4H, bpy 5/5', Ph ortho-H), 7.12 (br s, 3H, Ph meta-H, Ph-para H), 5.05 (br s, 1H, PhCHO) ppm.

^{1}H NMR (DMF-d_7, 500 MHz, 243 K): δ = 9.12 (d, J = 5.3 Hz, 1H), 8.85 (d, J = 5.45 Hz, 1H), 8.46 (d, J = 8.05 Hz, 1H), 8.30-8.27 (m, 2H), 8.12 (t, J = 7.85 Hz, 1H), 7.80 – 7.77 (m, 1H), 7.60 – 7.58 (m, 2H), 7.45 (t, J = 6.5 Hz, 1H), 7.09 (d, J = 5.2 Hz, 3H), 5.15 (s, 1H).

^{13}C-NMR (DMSO-d_6, 125 MHz, 298 K): δ = 153.50 (bpy 2/2'), 149.28 (bpy 6/6'), 135.79 (bpy 4/4'), 128.64 (Ph meta, Ph-para), 127.38 (bpy 5/5', Ph ortho), 122.21 (bpy 3/3'). -C-CHO and Ph-CHO are not observed.

IR: 1360 cm^{-1} (C–O streching)

Elemental analysis calculated for C$_{19}$H$_{16}$N$_2$Ni: C, 63.61; H, 4.40; N, 8.73. Found C, 60.20 ± 0.94; H, 4.38 ± 0.36; N, 8.01 ± 0.17.
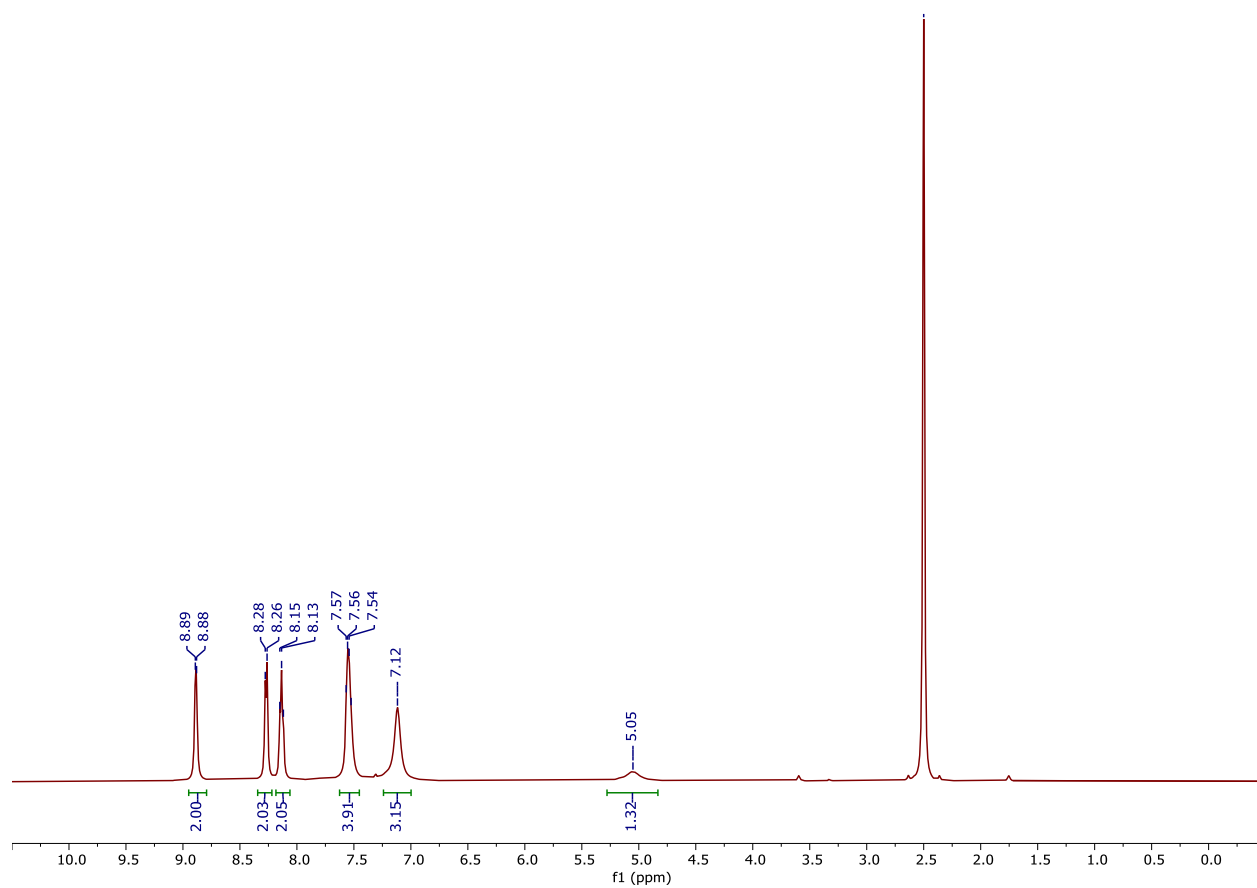
2.2. NMR spectroscopy

Figure S1. ^{1}H NMR spectrum of [Ni(bpy)(PhCHO)] (**2**) in DMSO-d_6.
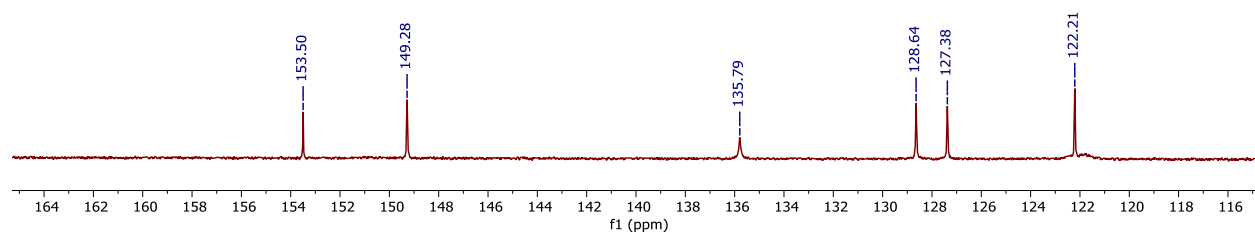
Figure S2. ^{13}C NMR spectrum of [Ni(bpy)(PhCHO)] (**2**) in DMSO-d_6.
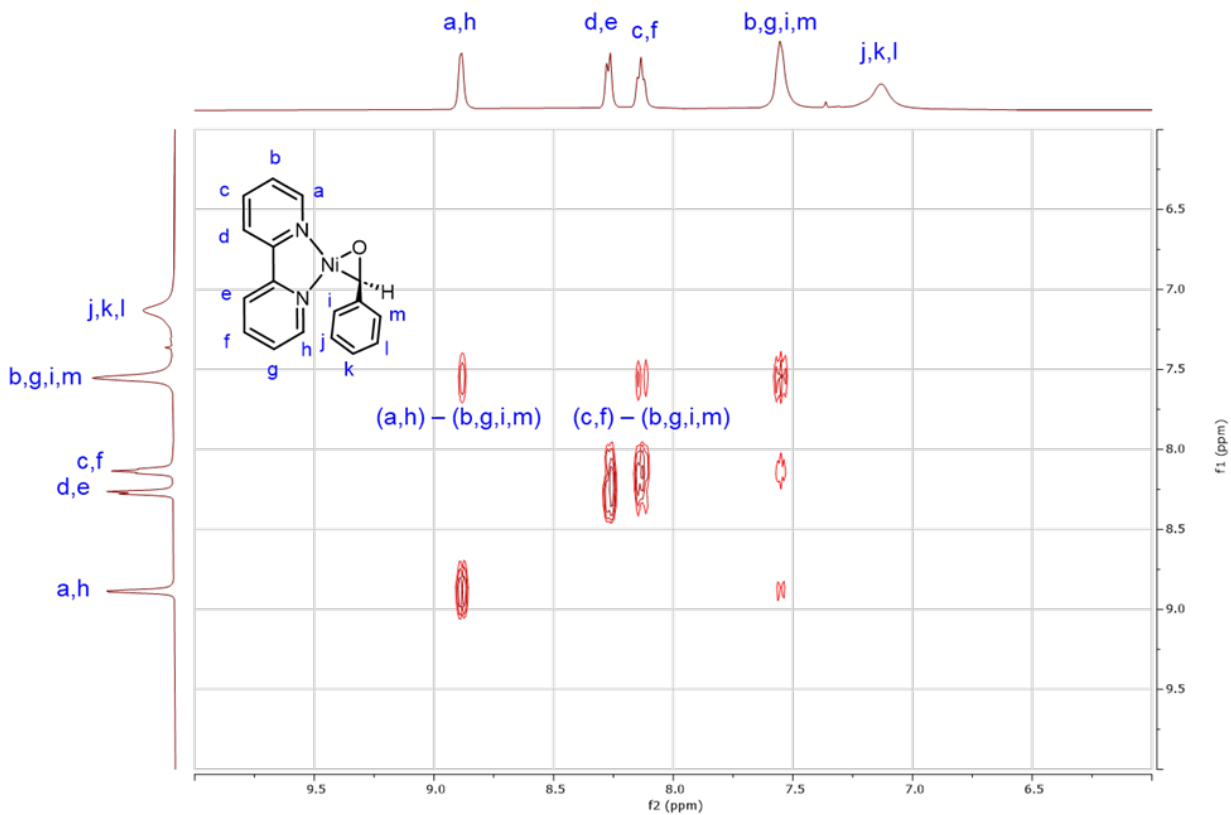
Figure S3. ^{1}H-^{1}H COSY NMR spectrum of [Ni(bpy)(PhCHO)] (**2**) in DMSO-d_6 (500 MHz).
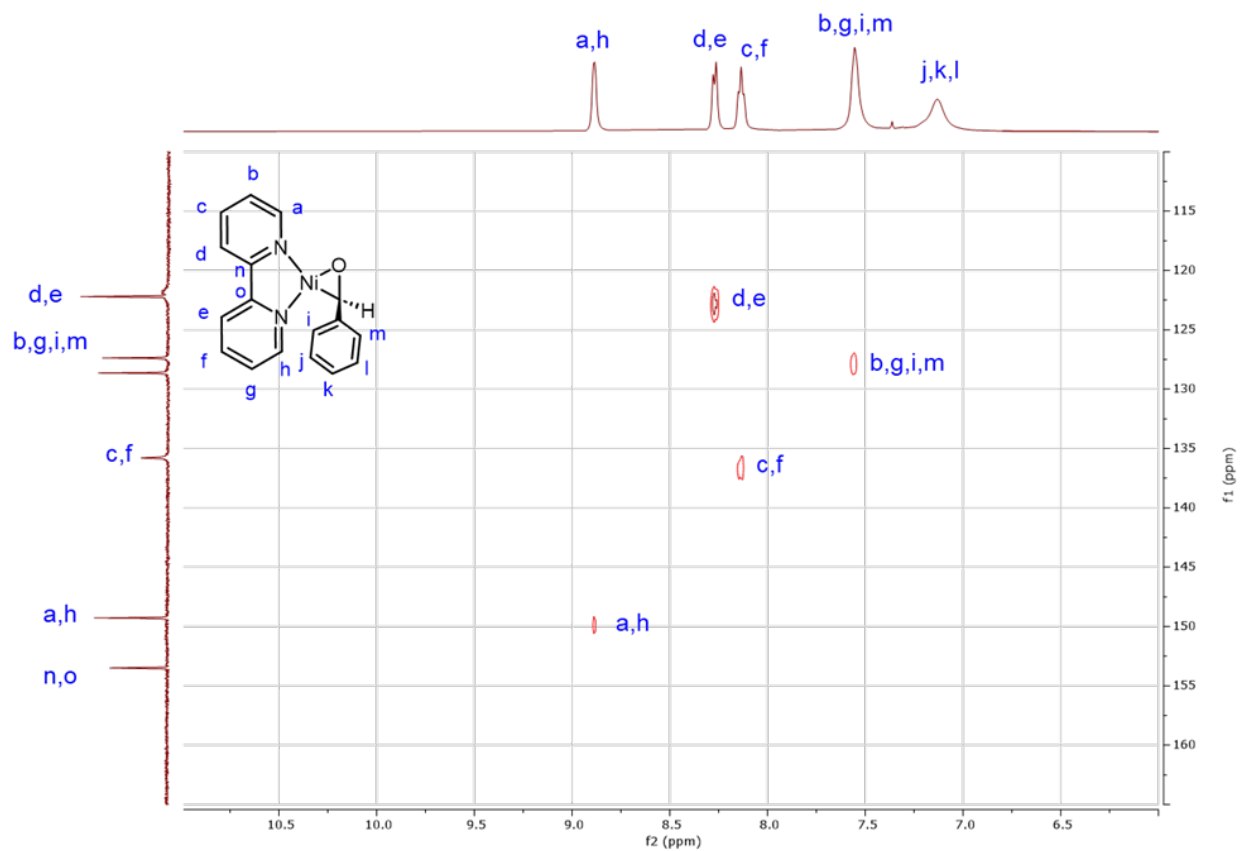
Figure S4. ^1H-^{13}C HSQC NMR spectrum of [Ni(bpy)(PhCHO)] (**2**) in DMSO-d_6 (500 MHz).

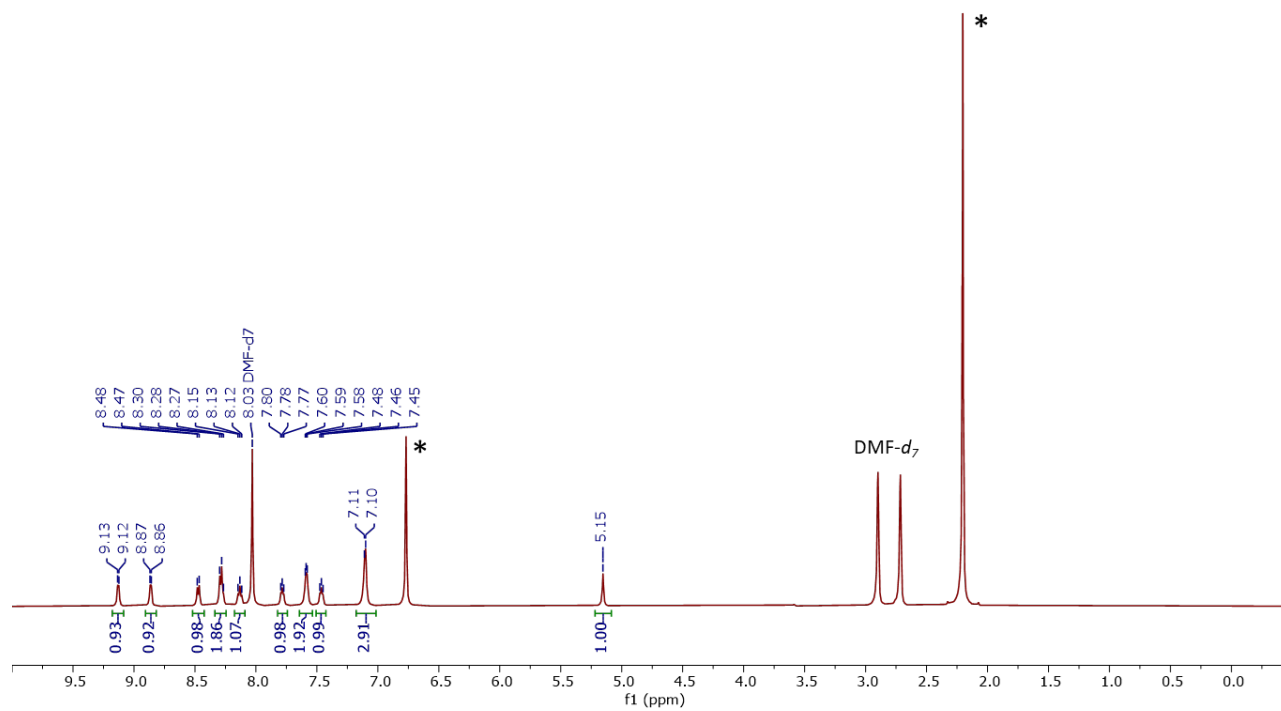**Figure S5.** ^{1}H NMR spectrum of [Ni(bpy)(PhCHO)] (**2**) in the presence of mesitylene* (internal standard) in DMF-d_7 at –30 °C (500 MHz).
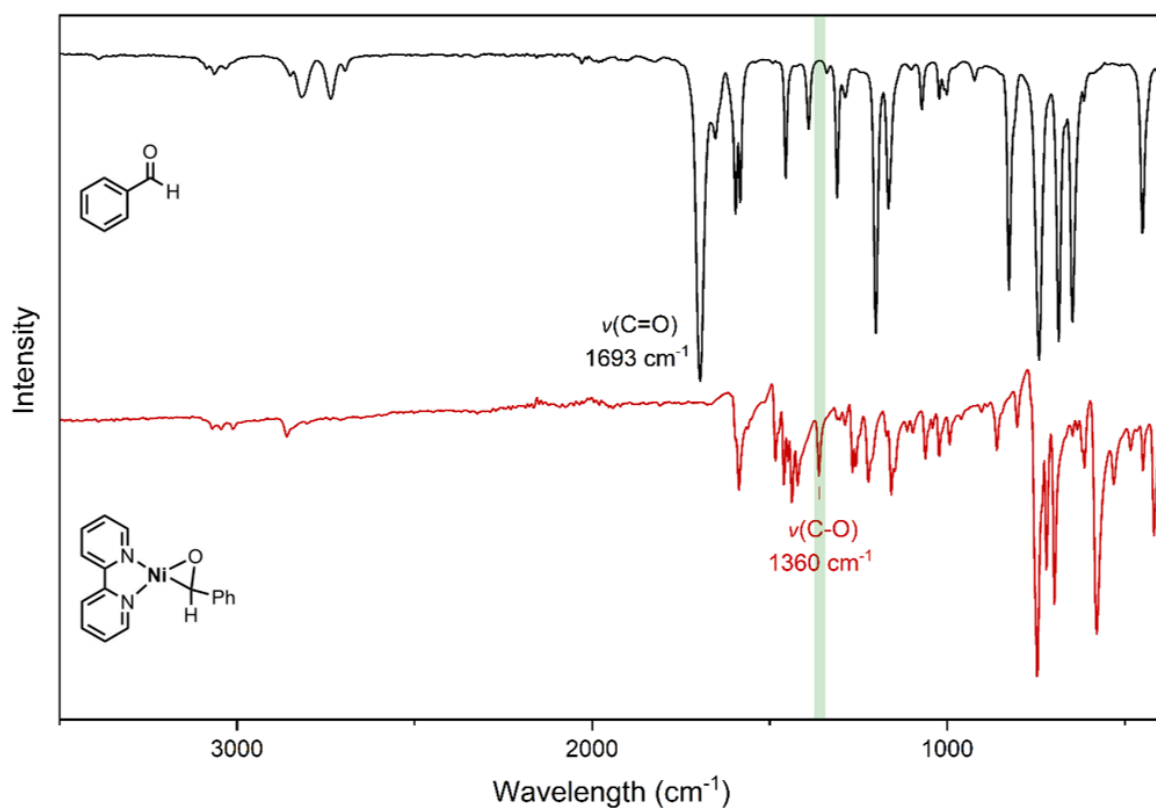
2.3. IR spectroscopy

Figure S6. IR spectra of **S1** (black) and **2** (red).

2.4. Crystallographic details for [Ni(bpy)(PhCHO)] (2)

In an Ar-filled glovebox, [Ni(COD)$_2$] (2.8 mg, 10 µmol, 1.0 eq.) and 2,2'-bipyridine (1.6 mg, 10 µmol, 1.0 eq.) were dissolved in 0.5 mL THF in an NMR tube. Benzaldehyde (1.0 µL, 10 µmol, 1.0 eq.) was dissolved in 1.5 mL pentane and the THF phase was overlaid with the pentane phase. After two weeks at room temperature, crystals suitable for single-crystal X-ray diffraction were obtained at the liquid-liquid interface.

A dark green single crystal of **2** was coated with perfluoropolyether at 230 Kelvin, picked up with a nylon loop and immediately mounted in the nitrogen cold stream of the diffractometers at 85 Kelvin. A Bruker D8 Venture diffractometer with Mo-target IµS3 X-ray source and INCOATEC focusing multilayer optics was used (Mo-Kα radiation; λ = 0.71073 Å).

A total of 3351 frames were collected. The total exposure time was 16.72 hours. The frames were integrated with the Bruker SAINT software package using a narrow-frame algorithm. The integration of the data using a monoclinic unit cell yielded a total of 88109 reflections to a maximum θ angle of 36.42° (0.60 Å resolution), of which 6709 were independent (average redundancy 13.133, completeness = 99.9%, R$_{int}$ = 4.43%, R$_{sig}$ = 2.01%) and 5923 (88.28%) were greater than 2σ(F^2). The final cell constants are based upon the refinement of the XYZ-centroids of 9985 reflections above 20 σ(I) with 4.969° < 2θ < 72.56°. Data were corrected for absorption effects using the Multi-Scan method (SADABS). The ratio of minimum to maximum apparent transmission was 0.911. The calculated minimum and maximum transmission coefficients (based on crystal size) are 0.9140 and 0.9330.

The final anisotropic full-matrix least-squares refinement on F2 with 193 variables converged at R1 = 2.93%, for the observed data and wR2 = 7.43% for all data. The goodness-of-fit was 1.066. The largest peak in the final difference electron density synthesis was 0.624 e-/Å^3 and the largest hole was -0.385 e-/Å^3 with an RMS deviation of 0.072 e-/Å^3. On the basis of the final model, the calculated density was 1.553 g/cm3 and F(000), 664 e$^-$. Crystal data collection and refinement details are given in Table S1.

Table S1. Crystallographic parameters for [Ni(bpy)(PhCHO)] (**2**).

CCDC deposition number	**2374778**
Identification code	**CEC0276_1**
Empirical formula	**C17 H14 N2 Ni O**
Formula weight	**321.01**
Temperature	**85(2) K**
Wavelength	**0.71073 Å**
Crystal system	**Monoclinic**
Space group	**P2(1)/n; No. 14**
a (Å)	**6.8635(3)**
b (Å)	**22.7679(9)**
c (Å)	**8.8158(3) Å**
α (deg)	**90**
β (deg)	**94.763(2)**
γ (deg)	**90**
Volume	**1372.87(9) Å3**
Z	**4**
Density (calculated)	**1.553 Mg/m3**
Absorption coefficient	**1.412 mm-1**
F(000)	**664**
Crystal size	**0.065 x 0.050 x 0.050 mm3**
Theta range for data collection	**2.48 to 36.42°.**
Index ranges	**-10<=h<=11, -38<=k<=38, -14<=l<=14**
Reflections collected	**88109**
Independent reflections	**6709 [R(int) = 0.0443]**
Completeness to theta = 25.24°	**99.9 %**
Absorption correction	**Semi-empirical from equivalents**
Max. and min. transmission	**0.93 and 0.91**
Refinement method	**Full-matrix least-squares on F2**
Data / restraints / parameters	**6709 / 0 / 193**
Goodness-of-fit on F2	**1.066**
Final R indices [I>2sigma(I)]	**R1 = 0.0293, wR2 = 0.0717**
R indices (all data)	**R1 = 0.0352, wR2 = 0.0743**
Largest diff. peak and hole	**0.624 and -0.385 e.Å-3**

3. Electrochemical experiments

All electrochemical experiments were performed in DMF 0.1 or 0.5 M nBu$_4$NPF$_6$ electrolyte solution at room temperature. An AgCl/Ag (leak-free type, OD of 5 mm, Innovative Instruments, Inc.) was used as reference electrode unless otherwise specified. The electrolyte and analyte mixtures were introduced in the electrochemical cell under Ar flow.

3.1. Cyclic voltammetry

Cyclic voltammograms (CVs) were recorded with a VSP-300 (Biologic Science Instruments, France) potentiostat equipped with an analogic ramp generator module. A glassy carbon disk (3 mm diameter, ALS Co., Ltd, Japan) and a coiled platinum wire (0.5 mm diameter, ALS Co., Ltd, Japan) were used as working and counter electrodes, respectively. The one-compartment electrochemical glass cells were filled with 5 mL of the electrolyte solution, and purged with Ar at least for 10 min. The working electrode was polished over an alumina polishing pad using a polishing alumina (0.05 µm, ALS Co., Ltd) followed by rinsing with deionized water and ethanol. Reference and counter electrodes were rinsed with ethanol. Electrode were dried under a stream of argon prior to insertion in the cell. After each CV measurements, the working electrode was taken from the cell and freshly polished. Unless otherwise noted, the CVs were recorded at a scan rate (v) of 0.1 V·s^{-1}. Ohmic drop compensation (85%) was applied. Reported potentials in CVs are referenced to the ferrocenium/ferrocene (Fc$^{+/0}$) couple (abbreviated to V$_{Fc}$) by adding ferrocene at the end of the measurements.

All CV experiments were performed in DMF 0.1 M nBu$_4$NPF$_6$ electrolyte solution with a concentration in **1** or **2** (when present) of 1 mM unless otherwise stated. In the case of **2**, CVs were conducted in the glovebox.

3.2. Electrolysis

Electrolysis were carried out using a SP-300 (Biologic Science Instruments, France) potentiostat. Electrolysis were performed in a customized H-type glass cell, having anode and cathode chambers separated by the glass frit (P3 pore size). A carbon foam (0.6 cm × 0.6 cm × 2.4 cm; VC003825, Goodfellow Cambridge Ltd, UK) and platinum mesh (20 x 20 mm, 0.1 mm thickness, Goodfellow Cambridge Ltd, UK) were used as working and counter electrodes, respectively.

Electrolysis of benzaldehyde (**S1**) in the presence of **1** and benzoic acid (BzOH) as proton source was conducted in 0.1 M nBu$_4$NPF$_6$ in DMF (see Manuscript Scheme 2A). The appropriate volume of electrolyte was introduced in each chamber of the electrochemical cell and sparged with Ar for 5 min. Right before electrolysis, the ohmic drop in the cell was determined. Then, electrolysis was performed under potentiostatic conditions, with no ohmic drop compensation applied. The cathodic electrolyte was continuously purged with Ar (ca. 1 mL·min^{-1}) during the run of electrolysis. Aliquots of ca 100 µL from the cathode chamber were collected during the electrolysis for analysis. Aliquots were analyzed by gas chromatography (GC) and by ^{1}H NMR spectroscopy, in which case 200 µL of aliquots were priorly mixed with 500 µL DMSO-d_6.

The bulk reductive electrolysis of a mixture of **1** and **S1** to generate **2** was carried out in DMF 0.5 M nBu$_4$NPF$_6$ in an Ar-filled glovebox (see Manuscript Scheme 2C).

3.3. Analytical method

Samples were analyzed by gas chromatography using a gas chromatograph equipped with a flame ionization detector (GC-FID; Nexis GC-2030, Shimadzu, Japan) with elution over a Rtx-1 column (30 m × 0.25 mm with 0.5 μm film t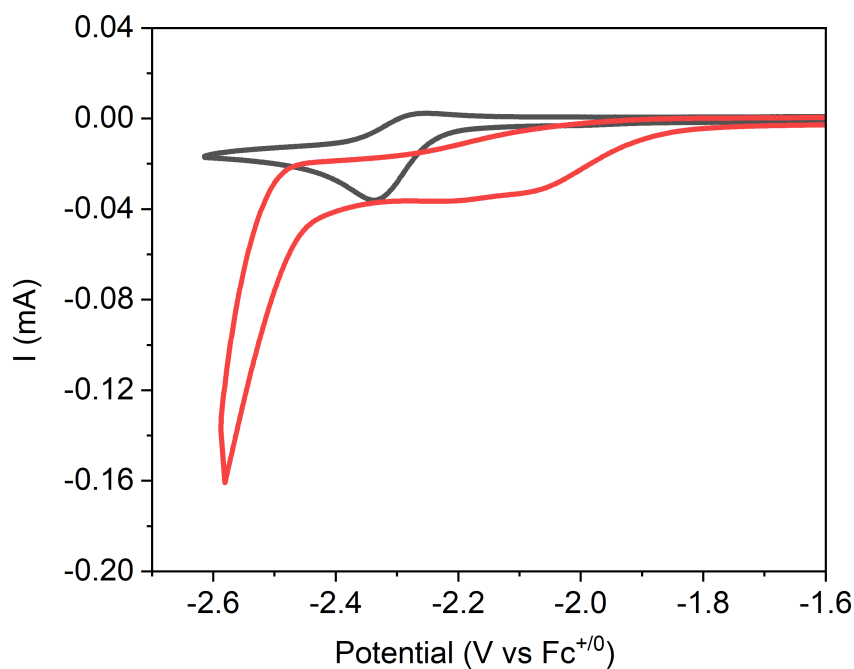hickness, Restek Corp., USA) using He as a carrier gas and a gas chromatograph equipped with a mass spectrometer (GC-MS; QP2020 NX, Shimadzu, Japan) with elution over a Rtx-1 column (30 m × 0.25 mm with 0.5 μm film thickness, Restek Corp., USA) using He as a carrier gas.

3.4. Additional CV data

Figure S7. CVs of **S1** (1mM) alone (black) and with BzOH (50 mM) (red).

2 displays a reversible reduction wave of halfwave potential $E_{1/2} = -2.06$ V_{Fc} (Figure S8). This value is in good agreement with the standard potential obtained from computation at $E°_{DFT}$ (**2/2⁻**) $= -2.14$ V_{Fc} (*vide infra* for computational details).
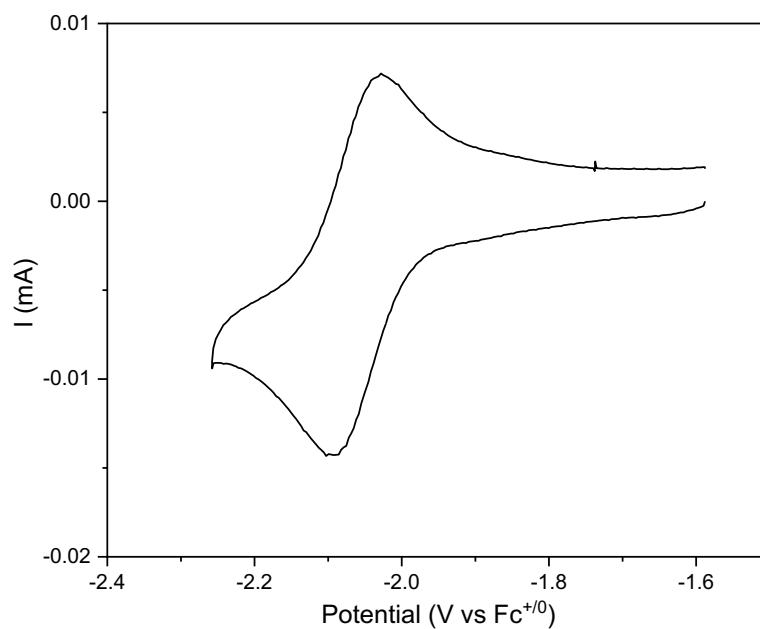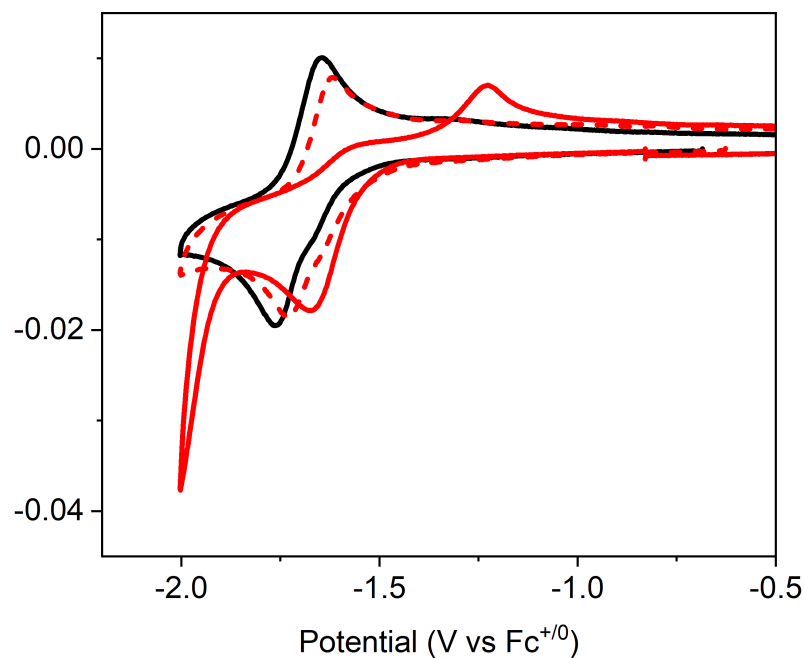

Figure S8. CV of **2**.

Figure S9. CVs of **1** (1 mM) alone (black), with BzOH (50 mM) (dotted red) and with BzOH (50 mM) and **S1** (1 mM) (red).

4. Stoichiometric experiments

4.1. Protonation of [Ni(bpy)(PhCHO)] (2)

In the glovebox, compound **2** (3.2 mg, 10 µmol, 1.0 eq.) was dissolved in 0.5 mL of deuterated solvent (DMSO-d_6 or DMF-d_7) in a J-Young NMR, followed by the addition of mesitylene (1.2 mg, 10 µmol, 1.0 eq.). The J-Young NMR tube was removed from the glovebox and analyzed using ^{1}H NMR to determine the initial amount of **2** in the solution. After the initial analysis, the tube was returned to the glovebox, where benzoic acid (2.4 mg, 20 µmol, 2.0 eq.) and tetrabutylammonium hexafluorophosphate (3.9 mg, 10 µmol, 1.0 eq.), when applicable, were added. The ^{1}H NMR analysis was performed after 0.5 h. Conversions and yields were calculated using mesitylene as an internal standard. Experiments with other H^{+} sources were conducted using the same procedure. H$_2$ yields are calculated on solution NMR data, not accounting for H$_2$ in the gas phase of the J-Young NMR tube, and therefore represent lower estimates.

Table S2. Stoichiometric experiments for protonation of [Ni(bpy)(PhCHO)] (**2**).

Entry	Substrate	H^{+} source	Solvent	pKa in MeCN	Additives	Conversion (%)	Yield (%)			
							S1H$_2$	S1$_2$H$_2$[a]	S1	H$_2$
1[b]	**S1**	BzOH	DMSO-d_6	21.5[3]	nBu$_4$NPF$_6$	<1	<1	<1	<1	<1
2	**2**	BzOH	DMSO-d_6	21.5	-	21	5	<1	<1	11
3	**2**	BzOH	DMSO-d_6	21.5	nBu$_4$NPF$_6$	26	5	<1	<1	11
4	**2**	PhOH	DMF-d_7	29.2[3]	nBu$_4$NPF$_6$	<1	<1	<1	<1	<1
5	**2**	BzOH	DMF-d_7	21.5	nBu$_4$NPF$_6$	21	4	<1	<1	6
6	**2**	[NEt$_3$H]BF$_4$	DMF-d_7	18.8[4]	nBu$_4$NPF$_6$	n.d.[c]	5	<1	<1	<1
7	**2**	C$_6$F$_5$CO$_2$H	DMF-d_7	18.8[d]	nBu$_4$NPF$_6$	>99	<1	2	97	<1
8	**2**	[lutH]BF$_4$	DMF-d_7	14.1[4]	nBu$_4$NPF$_6$	>99	19	15	36	2
9	**2**	[PhNH$_3$]BF$_4$	DMF-d_7	10.6[4]	nBu$_4$NPF$_6$	>99	6	24	<1	4
10	**2**	[DMFH]OTf	DMF-d_7	6.1[5]	nBu$_4$NPF$_6$	>99	<1	37	<1	6
11	**2**	BzOH[e]	DMF-d_7	21.5	nBu$_4$NPF$_6$	>99	3	<1	12	6
12	**2**	BzOD	DMF-d_7	21.5	nBu$_4$NPF$_6$	40	<1	<1	<1	<1

[a]Theoretical maximal yield 50%. [b]Control experiment in absence of **2**. [c]Accurate quantification of remaining **2** was not possible due to spectral overlaps. [d]pKa was calculated following ref[6]. [e]10 equivalents BzOH.

The absence of traceable amounts of products in ^{1}H NMR when deuterated BzOD is used instead of BzOH supports that the protons in the hydrogenation product **S1**H$_2$ originate from the acid introduced (compare Entries 5 and 12 in Table S2.)
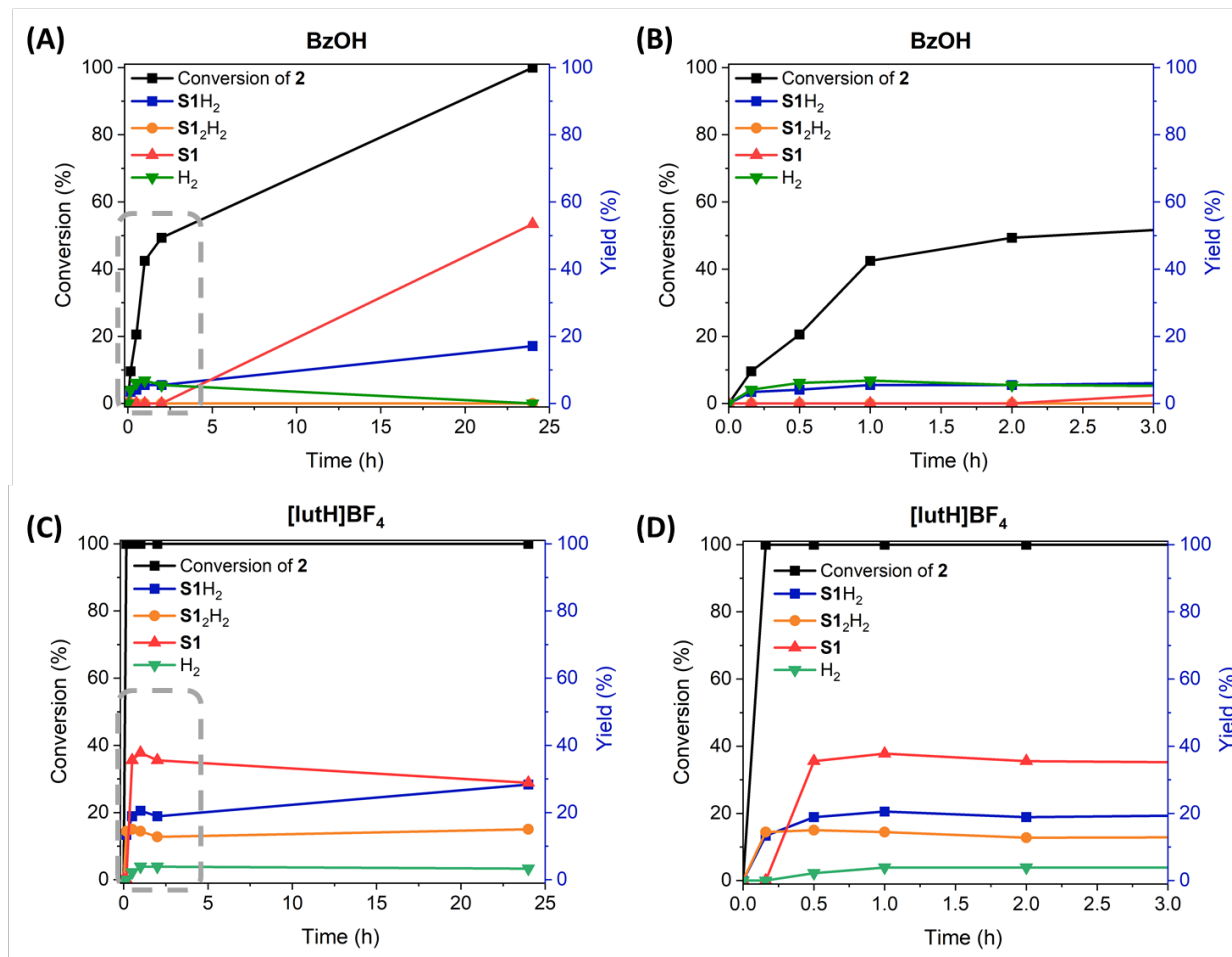

Figure S10. Time-profiles for stoichiometric protonation experiments with [Ni(bpy)(PhCHO)] (**2**). Reaction with benzoic acid (BzOH, Entry 5 in Table S2) (A) and magnification of the first 2 hours (B). Reaction with [2,6-Lutidinium]BF$_4$ ([lutH]BF$_4$, Entry 8 in Table S2) (C) and magnification of the first 2 hours (D).
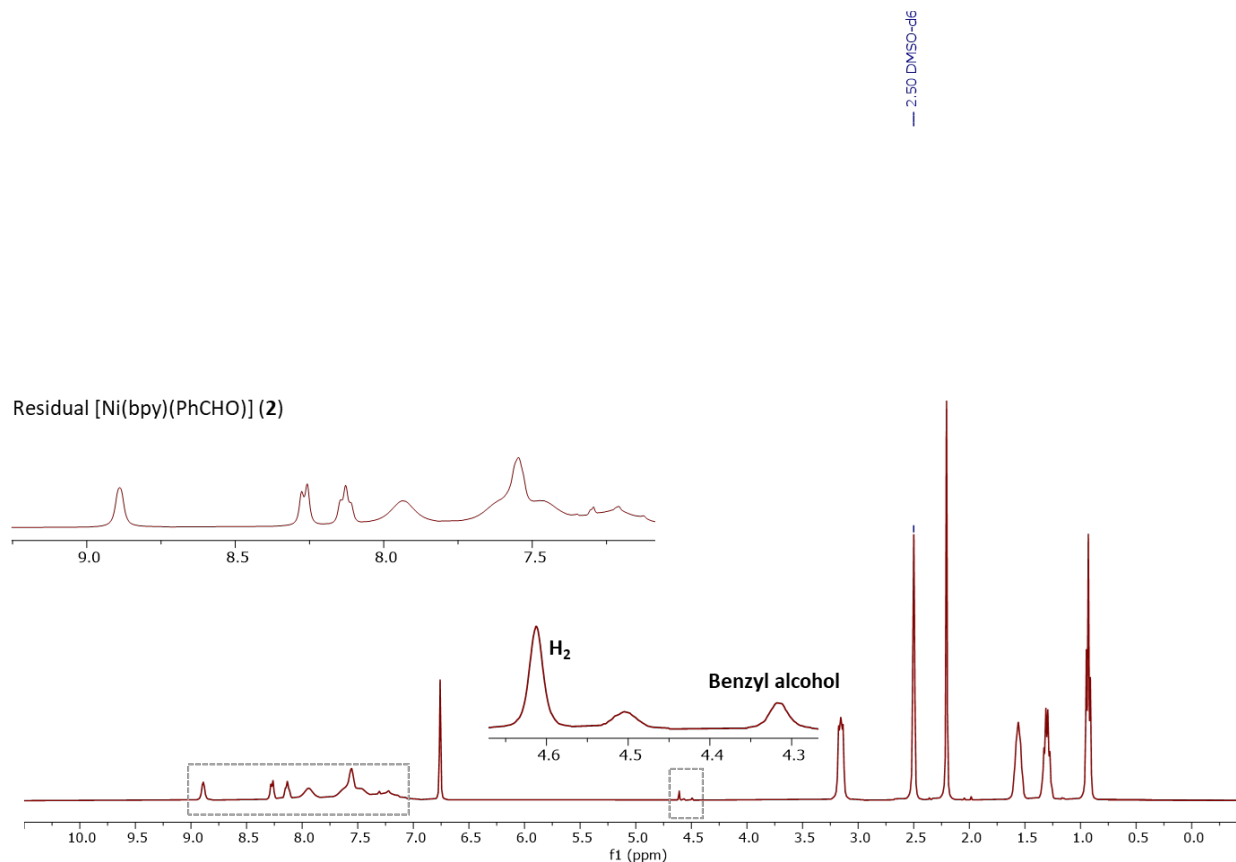
Figure S11. ^{1}H NMR spectrum of the crude mixture of Entry 2 in Table S2 (DMSO-d_6).
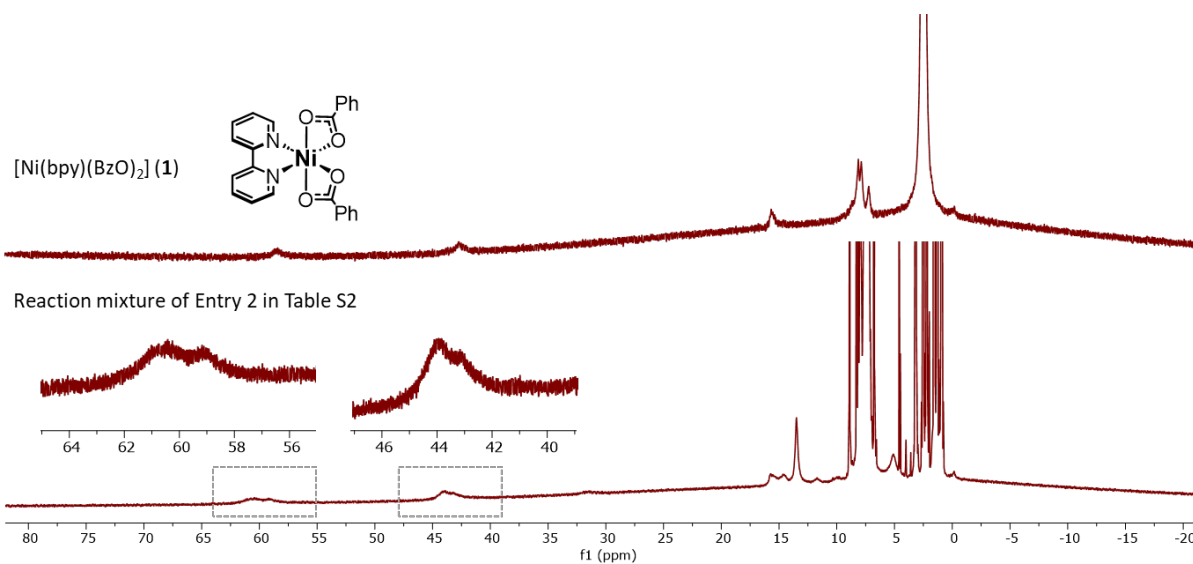
Figure S12. ^{1}H NMR spectrum of the crude mixture of Entry 2 in Table S2 (bottom) and of **1** (top) (DMSO-d_6).
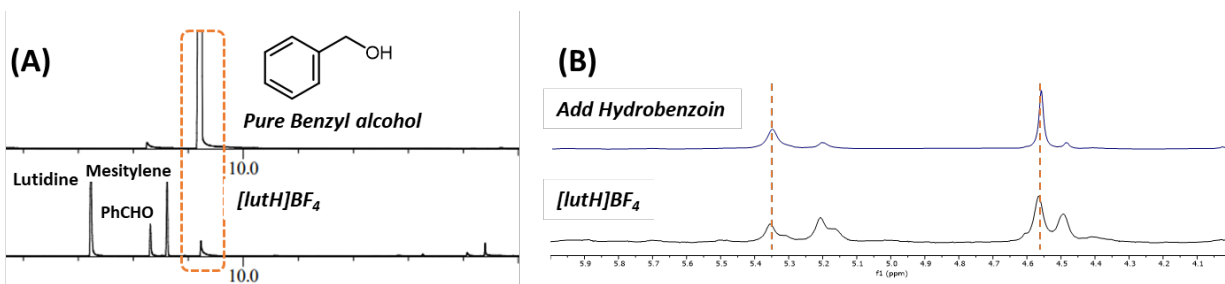
Figure S13. Analysis of stoichiometric protonation experiment of **2** with [lutH]BF₄: (A) GC-MS chromatogram of the crude mixture (bottom) and comparison with pure benzyl alcohol (top) and (B) ¹H NMR spectra of the crude mixture (black) and after addition of hydrobenzoin (blue).
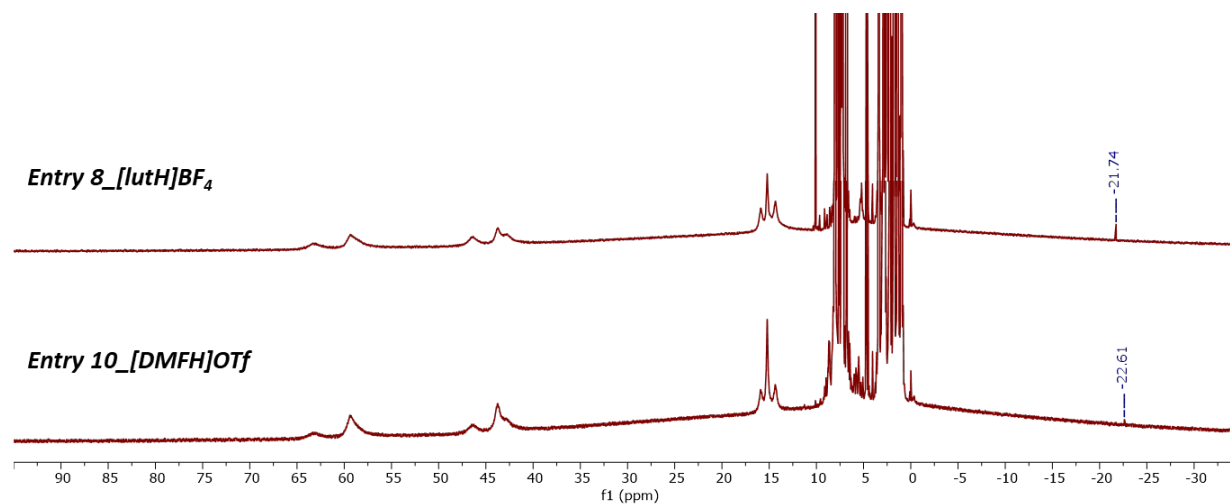
Figure S14. ¹H NMR spectrum of the crude mixture of Entry 8 and 10 in Table S2.

4.2. Reactivity of [Ni(bpy)(PhCHO)] (2) with Lewis acids

Table S3. Stoichiometric experiments with **2** and Lewis acids.

Entry	Substrate	Lewis acids	Solvent	Additives	Conversion (%)	Yield (%)		
						$S1H_2$	$S1_2H_2$	S1
1	**2**	TMSOTf	DMSO-d_6	nBu$_4$NPF$_6$	>99	<1	<1	13
2	**2**	[Sc(OTf)$_3$]	DMSO-d_6	nBu$_4$NPF$_6$	66	<1	<1	<1
3	**2**	BEt$_3$[a]	DMSO-d_6	nBu$_4$NPF$_6$	<1	<1	<1	<1

[a]Triethylborane solution 1.0 M in hexane.

4.3. Reactivity of [Ni(OMebpy)(PhCHO)]

[Ni(OMebpy)(PhCHO)] was prepared following the same procedure as for **2** but using 4,4-dimethoxy-2,2'-bipyridine instead of 2,2'-bipyridine.

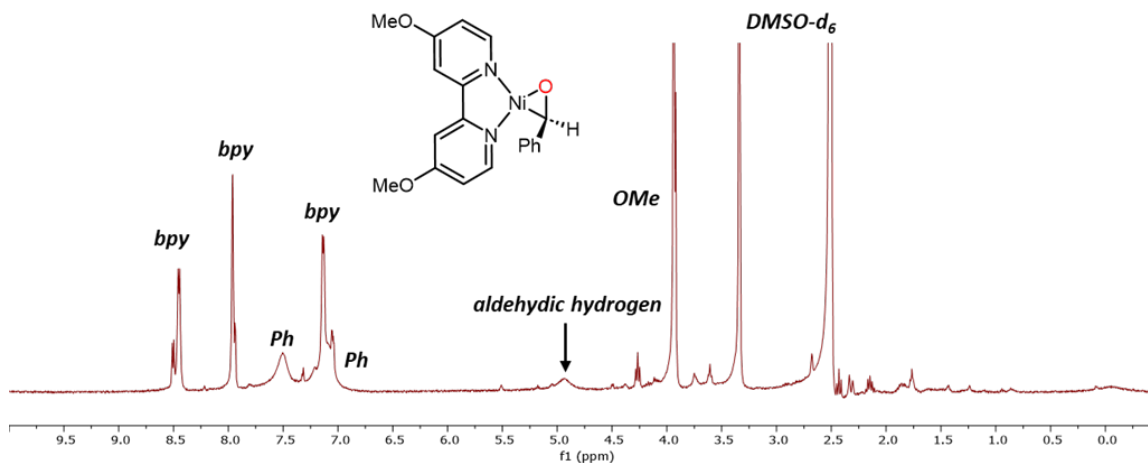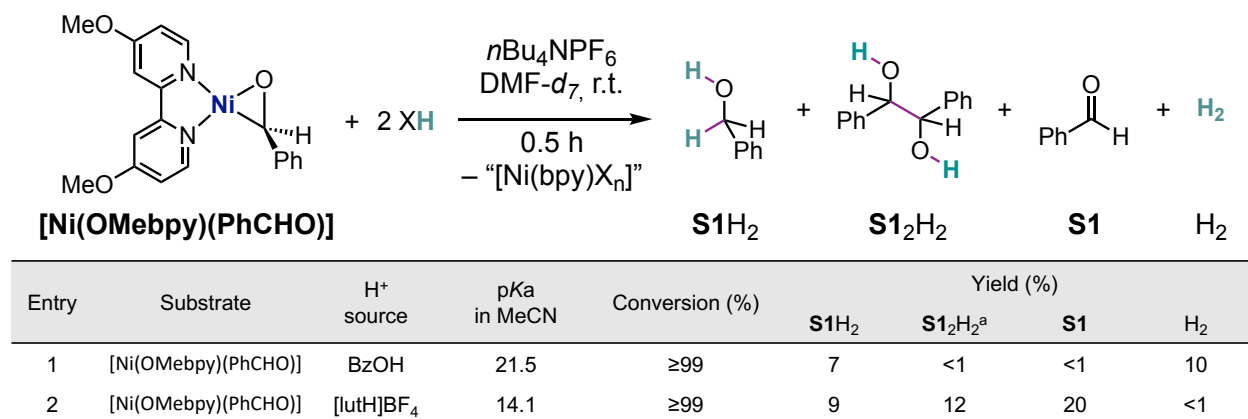**Figure S15.** ^1H spectrum of [Ni(OMebpy)(PhCHO)] (DMSO-d_6).

Table S4. Stoichiometric protonation experiments with [Ni(OMebpy)(PhCHO)].

Entry	Substrate	H+ source	pKa in MeCN	Conversion (%)	Yield (%)			
					$S1H_2$	$S1_2H_2{}^a$	S1	H_2
1	[Ni(OMebpy)(PhCHO)]	BzOH	21.5	≥99	7	<1	<1	10
2	[Ni(OMebpy)(PhCHO)]	[lutH]BF$_4$	14.1	≥99	9	12	20	<1

^{a}Theoretical maximal yield 50%.

4.4. Electrochemical stoichiometric experiments

The formation of **2** under electrochemical conditions was conducted in the glovebox. The electrolysis was run with [Ni(bpy)(OBz)$_2$] (**1**; 10 mM) and benzaldehyde (**S1**; 10 mM) at $E_{app} = -1.80$ V$_{Fc}$ until the current shows saturation ($Q_f = -4.56$ C; ca 1e$^-$/**1**). After the electrolysis, CV was performed and the first reduction wave (**2→2$^-$**) and the first reoxidation wave (**2→2$^+$**) are consistent with the CV of the isolated complex **2**, further supporting the electrogeneration of **2**.
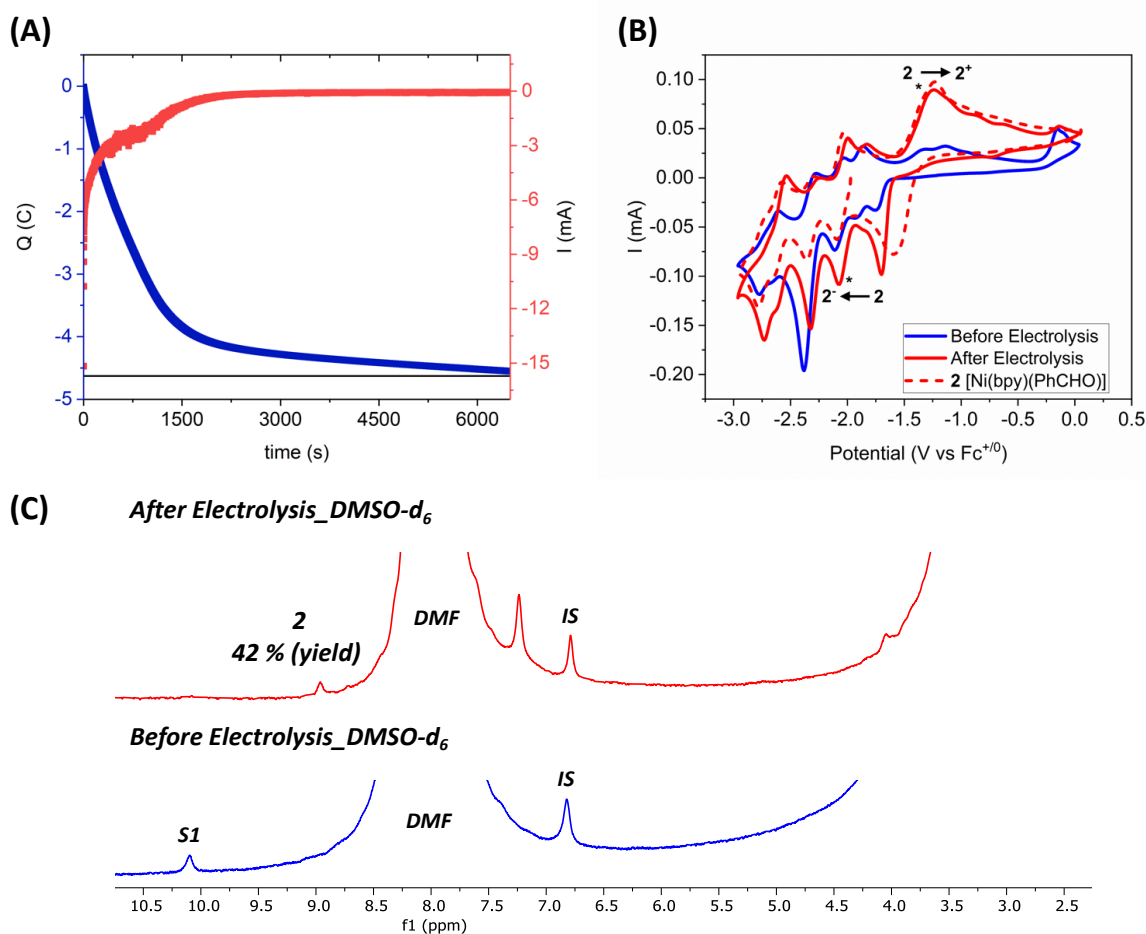
Figure S16. (A) Charge (blue) and current (red) vs. time during electrolysis of a mixture of compound **1** (10 mM) and **S1** (10 mM) at $E_{app} = -1.80$ V$_{Fc}$. (B) CVs recorded prior to electrolysis (blue) and post-electrolysis (red) and of **2** alone (1 mM) (red dotted); * indicate events attributed to the **2/2$^-$** and **2$^+$/2** couples. (C) ^{1}H NMR spectra acquired before electrolysis (blue) and after electrolysis (red).

5. Computational details

5.1. General considerations

Calculations were performed using the ORCA 5.0 suite of software.[7] The PBE0 functional[8] with Grimme's D3BJ dispersion correction[9] was used in conjunction with the 6-311+G(d,p) basis set for all atoms.[10-14] All geometries were fully optimized without any symmetry or geometry constraints. Harmonic vibrational analyses were performed to confirm and characterize the structures as minima or transition states. Free energies were calculated within the harmonic approximation for vibrational frequencies. Unless otherwise stated, the spin configurations of the nickel complexes in this study are calculated in the singlet ground state and the doublet ground state for the open-shell nickel(I) complexes. The effects of the solvation by DMF were included in the energy calculations using the C-PCM model.[15] Standard potentials were calculated with respect to the phenazine$^{0/-}$ redox couple and converted back versus the Fc$^{+/0}$ redox couple as previously described for accuracy.[16]
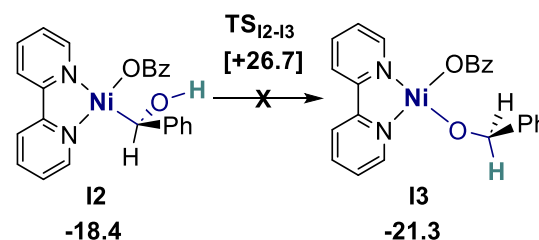
5.2. Additional computational results

Further protonation or isomerisation processes from **I2** (Figure S17) have been discarded based on associated high energy TSs ($\Delta\Delta G^{\ddagger} > +40$ kcal mol^{-1}).
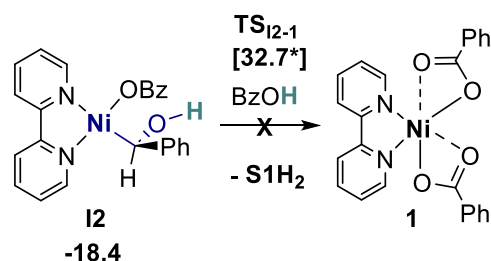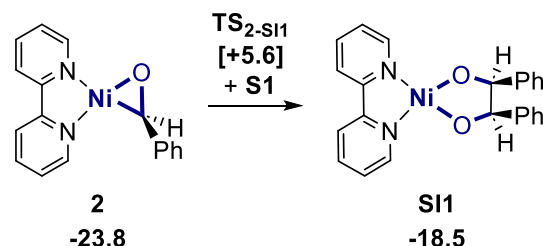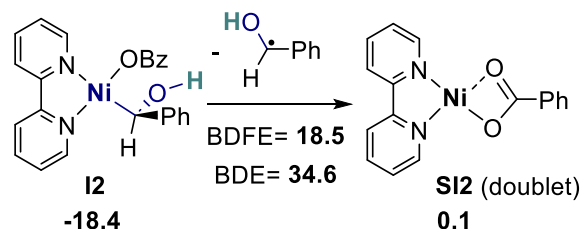

Figure S17. Gibbs free energy (kcal mol^{-1}) for additional pathways computed at PBE-D3/6-311+G(d,p) level of theory and CPCM model to account for solvent effect (DMF) using **I1** as thermodynamic reference. *Two imaginary frequencies.

Table S5. Computed and experimental redox potentials.

Transition	E (V_{Fc})	
	Computed	Experimental
2$^{+/0}$	−1.36	−1.29
2$^{0/−}$	−2.14	−2.06
I2$^{0/−}$	−1.21	-
I3$^{0/−}$	−1.45	-

5.3. Three lowest frequencies and Gibbs free energy for all computed structures

Structures relevant for the HER pathway and SI2 (see Scheme 3 in the main text) have already been reported by our group.[1] Structure geometries can be found in the xyz document attached.

S1


```
        109.34 cm**-1
        213.74 cm**-1
        226.92 cm**-1
Final Gibbs free energy        ...   -345.18471925 Eh
```
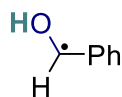
S1H$_2$
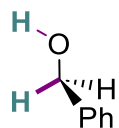

```
         32.03 cm**-1
        133.34 cm**-1
        239.55 cm**-1
Final Gibbs free energy        ...   -346.35940506 Eh
```

S1H$^•$

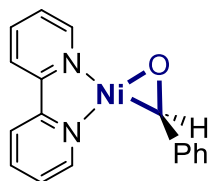```
        133.61 cm**-1
        204.04 cm**-1
        228.72 cm**-1
Total Enthalpy   ...   -345.70139292 Eh
Final Gibbs free energy   ...   -345.74092190 Eh
```
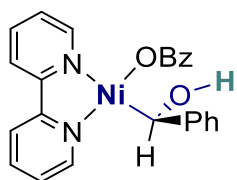
**2**



```
        19.32 cm**-1
        26.10 cm**-1
        49.03 cm**-1
Final Gibbs free energy   ...   -2348.11194894 Eh
```
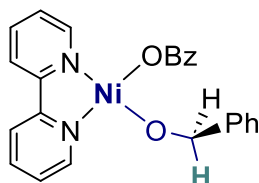
**I2**



```
        14.81 cm**-1
        20.23 cm**-1
        22.39 cm**-1
Final Gibbs free energy        ...   -2768.49696294 Eh
```

I3


```
         2.67 cm**-1
        18.03 cm**-1
        23.10 cm**-1
Final Gibbs free energy        ...   -2768.50154148 Eh
```

I4
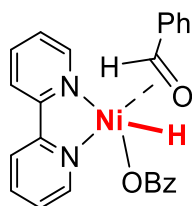

```
         9.72 cm**-1
        15.67 cm**-1
        24.65 cm**-1
Final Gibbs free energy        ...   -2768.46760236 Eh
```

SI1
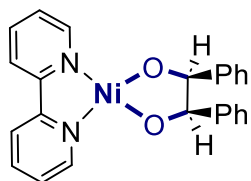

```
        20.41 cm**-1
        20.73 cm**-1
        27.94 cm**-1
Final Gibbs free energy        ...  -2693.29115923 Eh
```

SI2[1]

```
Total Enthalpy                 ...  -2422.66384625 Eh
```

TS_I1-2
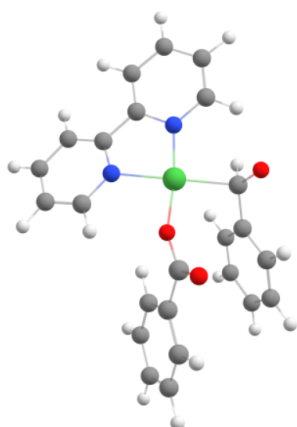

```
       -41.14 cm**-1 ***imaginary mode***
        12.87 cm**-1
        23.03 cm**-1
Final Gibbs free energy        ...  -2768.01435965 Eh
```

TS_2-I2
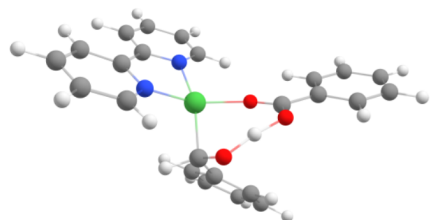

```
      -538.66 cm**-1 ***imaginary mode***
         6.14 cm**-1
        17.17 cm**-1
Final Gibbs free energy        ...  -2768.48602419 Eh
```

TS_{2-I3}
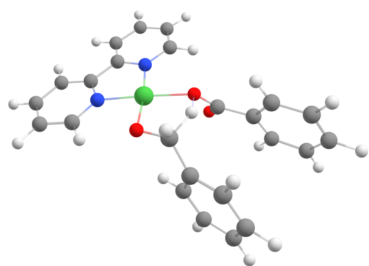

```
      -717.64 cm**-1 ***imaginary mode***
        15.43 cm**-1
        19.65 cm**-1
Final Gibbs free energy         ...  -2768.46385387 Eh
```

TS_{I2-1}
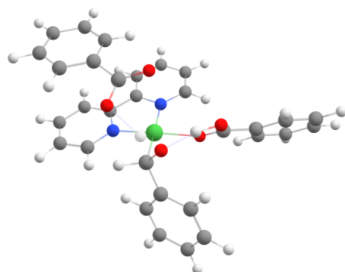

```
      -692.14 cm**-1 ***imaginary mode***
       -59.70 cm**-1 ***imaginary mode***
        10.95 cm**-1
Final Gibbs free energy         ...  -3188.81211283 Eh
```

TS_{I3-1}
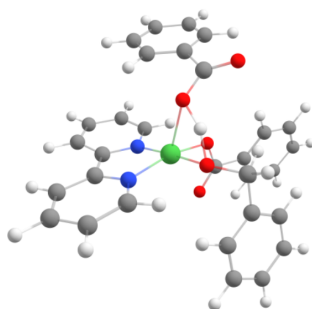

```
      -652.96 cm**-1 ***imaginary mode***
         4.37 cm**-1
        16.23 cm**-1
Final Gibbs free energy         ...  -3188.87262525 Eh
```

TS_{I2-I3}
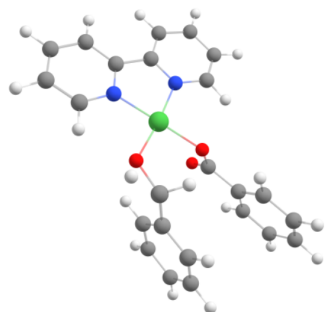

```
      -1444.74 cm**-1 ***imaginary mode***
          8.06 cm**-1
         26.16 cm**-1
Final Gibbs free energy        ...  -2768.42504558 Eh
```

TS_{I2-I4}
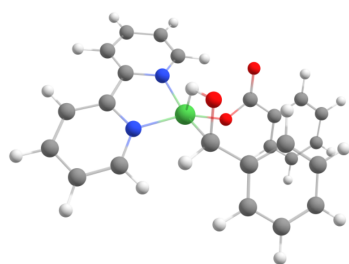

```
       -187.58 cm**-1 ***imaginary mode***
         13.23 cm**-1
         19.22 cm**-1
Final Gibbs free energy        ...  -2768.45332454 Eh
```

TS_{I3-I4}
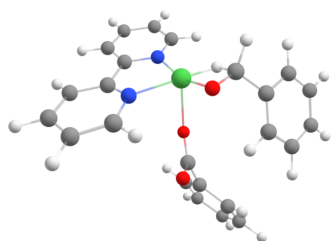

```
       -201.31 cm**-1 ***imaginary mode***
          6.20 cm**-1
         18.31 cm**-1
Final Gibbs free energy        ...  -2768.43664544 Eh
```
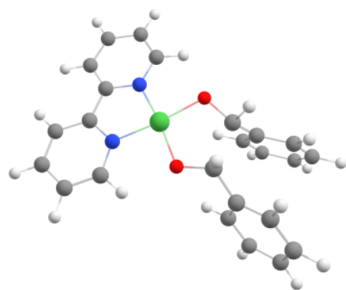
TS_{I4-IH}
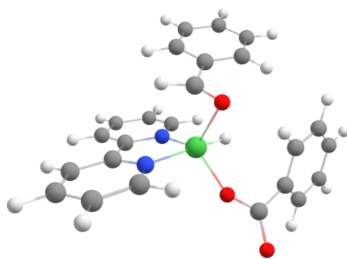

```
        -83.21 cm**-1 ***imaginary mode***
         14.53 cm**-1
         18.36 cm**-1
Final Gibbs free energy        ...  -2768.46442056 Eh
```

TS_{2-SI1}


```
        -201.60 cm**-1 ***imaginary mode***
         12.03 cm**-1
         17.94 cm**-1
Final Gibbs free energy        ...  -2693.25273639 Eh
```

6. References

1. G. Durin, M.-Y. Lee, M. A. Pogany, T. Weyhermüller, N. Kaeffer and W. Leitner, *J. Am. Chem. Soc.*, 2023, **145**, 17103-17111.

2. E. Dinjus, H. Langbein and D. Walther, *J. Organomet. Chem.*, 1978, **152**, 229-237.

3. A. Kütt, S. Tshepelevitsh, J. Saame, M. Lõkov, I. Kaljurand, S. Selberg and I. Leito, *Eur. J. Org. Chem.*, 2021, **2021**, 1407-1419.

4. B. D. McCarthy and J. L. Dempsey, *Inorg. Chem.*, 2017, **56**, 1225-1231.

5. A. Le Goff, V. Artero, B. Jousselme, P. D. Tran, N. Guillet, R. Metaye, A. Fihri, S. Palacin and M. Fontecave, *Science*, 2009, **326**, 1384-1387.

6. E. Rossini, A. D. Bochevarov and E. W. Knapp, *ACS Omega*, 2018, **3**, 1653-1662.

7. F. Neese, *WIREs Comput. Mol. Sci.*, 2022, **12**, e1606.

8. C. Adamo and V. Barone, *J. Chem. Phys.*, 1999, **110**, 6158-6170.

9. S. Grimme, S. Ehrlich and L. Goerigk, *J. Comput. Chem.*, 2011, **32**, 1456-1465.

10. R. Krishnan, J. S. Binkley, R. Seeger and J. A. Pople, *J. Chem. Phys.*, 1980, **72**, 650-654.

11. L. A. Curtiss, M. P. McGrath, J. P. Blaudeau, N. E. Davis, R. C. Binning and L. Radom, *J. Chem. Phys.*, 1995, **103**, 6104-6113.

12. T. Clark, J. Chandrasekhar, G. W. Spitznagel and P. V. R. Schleyer, *J. Comput. Chem.*, 1983, **4**, 294-301.

13. M. J. Frisch, J. A. Pople and J. S. Binkley, *J. Chem. Phys.*, 1984, **80**, 3265-3269.

14. F. Weigend, *Phys. Chem. Chem. Phys.*, 2006, **8**, 1057-1065.

15. M. Cossi, N. Rega, G. Scalmani and V. Barone, *J. Comput. Chem.*, 2003, **24**, 669-681.

16. J. J. Moreno, S. L. Hooe and C. W. Machan, *Inorg. Chem.*, 2021, **60**, 3635-3650.

7. Author contributions

Conceptualization: G.D. and N.K.; funding acquisition: W.L.; investigation: G.D., M.L., M.A.P., C.K. and T.W.; project administration: N.K.; supervision: G.D. and N.K.; writing – original draft: G.D. and N.K; writing – review & editing: G.D., M.L., M.A.P., C.K., T.W., W.L. and N.K.